ARTICLE

fib WILEY

Flexural behavior and minimum reinforcement condition in hybrid-reinforced concrete beams

Alessio Rubino[1] ⓘ | **Federico Accornero**[2] ⓘ | **Alberto Carpinteri**[1,3]

[1]DISEG, Politecnico di Torino, Turin, Italy

[2]College of Engineering, Shantou University, Shantou, China

[3]Department of Civil and Environmental Engineering, Shantou University, Shantou, China

Correspondence
Alessio Rubino, DISEG, Politecnico di Torino, Turin, Italy.
Email: alessio.rubino@polito.it

Abstract

Hybrid reinforced concrete (HRC) can be defined as a cementitious material in which the reinforcing secondary phase consists of a combination of continuous steel rebars and of short discontinuous fibers, randomly distributed within the concrete matrix. For these structural elements, experimental flexural tests highlight how the postcracking response of the composite is strongly affected by the amount of steel bars together with reinforcing fibers. In the present work, it is shown that the action of these two contributions can be clearly interpreted in the framework of Fracture Mechanics through the Updated Bridged Crack Model (UBCM). The model assumes nonlinear constitutive laws to describe the toughening action of the reinforcing secondary phases, which are related to the yielding of steel rebars and to the pull-out of the short fibers. Under these assumptions, different postcracking regimes depending on three scale-dependent dimensionless numbers can be predicted: the *bar-reinforcement brittleness number*, N_P, which is directly related to the steel bar area percentage, ρ; the *fiber-reinforcement brittleness number*, $N_{P,f}$, which is directly related to the fiber volume fraction, V_f; and the *pull-out brittleness number*, N_w, which depends on the critical embedment length of the fiber-reinforcement, w_c. The couples of critical values of the two reinforcement brittleness numbers define the minimum reinforcement conditions of the HRC structural element—that is, the combination of ρ_{min} and $V_{f,min}$ required to guarantee a stable post-cracking response—including its scale dependence. A parametrical analysis is presented together with the modeling of an experimental campaign reported in the literature in order to assess the effectiveness of the UBCM.

KEYWORDS
hybrid-reinforced concrete, minimum reinforcement, scale effects, updated bridged crack model

1 | INTRODUCTION

During the last 40 years, an extensive research work has focused onto the beneficial influence of reinforcing fibers on the mechanical behavior of cementitious composites. It is relevant whether the fibers represent a single reinforcing phase—that is, in the case of fiber-reinforced concrete (FRC) elements—or they represent a supplementary reinforcement in addition to the traditional steel-bars, leading to the definition of the so-called *hybrid-reinforced concrete* (HRC).

In the case of FRC, it is widely acknowledged that the fibers provide an improvement of the mechanical properties of the composite with respect to plain concrete, including fracture energy, tensile, compressive, and shear strengths. Several experimental investigations evidenced that the contribution of the reinforcing fibers depends on several factors, among which: (i) the fiber volume fraction, V_f[1,2]; (ii) the mechanical and geometrical properties of the reinforcing fibers (tensile strength, geometric profile, and aspect ratio) and of the cementitious matrix (mainly, its compression strength)[3,4]; (iii) the specimen sizes[5]; (iv) the fiber distribution within the volume of the composite.[6]

In the case of HRC, the influence of the fibers should be discussed by taking into account the interaction with ordinary bar reinforcement. Considering an HRC beam subjected to bending, the flexural behavior up to failure depends, among other parameters, on the amount of reinforcement, that is, the steel-bar reinforcement ratio, ρ, together with the fiber volume fraction, V_f (Figure 1). In the case of low steel-bar reinforcement ratio, that is, lightly-

reinforced concrete beams, the flexural response is characterized by a plastic plateau due to the yielding of the longitudinal steel-bars (see lower curves in Figure 1). Under these circumstances, the addition of fibers provides an increase in the load-bearing capacity of the specimen,[7] together with a variation in the deflection capacity, which is found to be reduced or increased depending on the amount of longitudinal steel bars. For very low reinforcement ratio, several experimental investigations pointed out the reduction in the deflection capacity of the HRC specimens in comparison to the case of RC beams without fibers.[8,9] This effect is related to the beneficial influence of fibers on the bond behavior at the concrete-bar interface, which does not allow the yielded steel bar to develop plastic deformation, thus promoting crack localization and early tensile failure of the bar.[10,11] On the other hand, this phenomenon may not be observed when the steel-bar reinforcement ratio is sufficient to develop the gradual strain-hardening of the bar, which is found to be enhanced by the presence of short fibers, leading to an increase in the ultimate deflection of the specimen.[7,12,13]

Considering an over-reinforced concrete beam, the plastic plateau is followed by crushing (compression damage) of concrete, which leads to the final failure of the beam (see upper curves in Figure 1). In this case, the addition of fiber has a negligible influence on the load bearing capacity, considering that the major contribution is given by the ordinary reinforcement. On the other hand, the fibers strongly affect the crushing branch of the response, which becomes significantly more gradual.[12,14] This is due to the confinement action of the short fibers
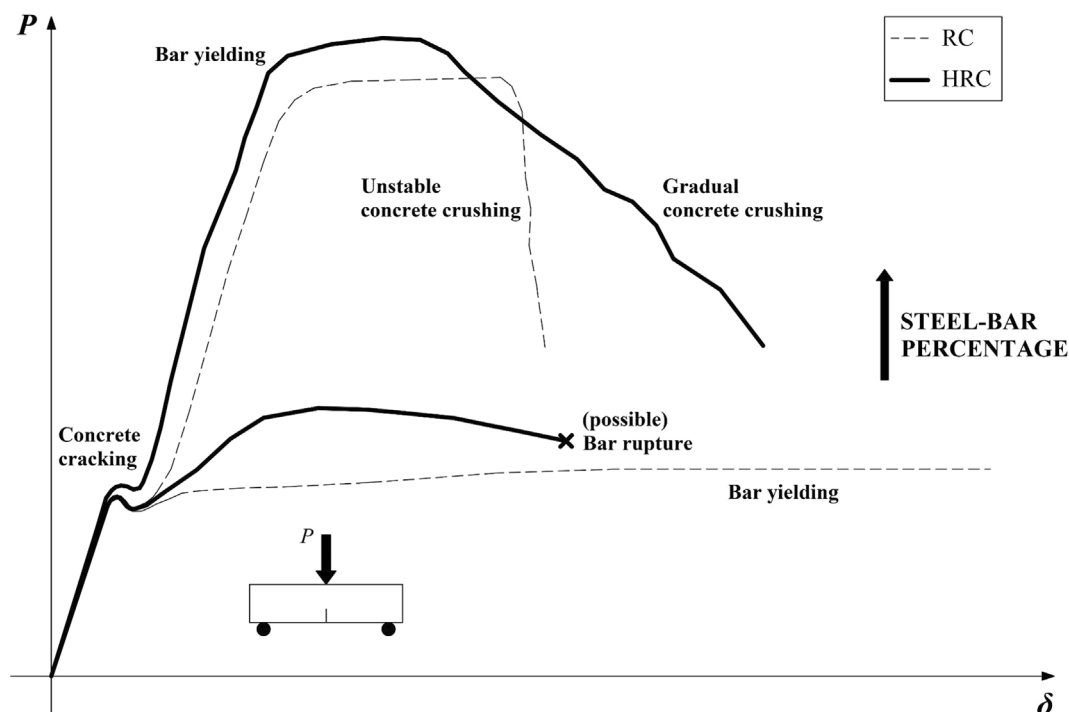

FIGURE 1 Influence of fiber addition on the flexural response of lightly and over-reinforced concrete beams.

that, in close analogy to the transverse reinforcement (stirrups), enhances the concrete crushing energy.[15–17]

Due to the large number of variables affecting the phenomenon, the FRC mechanical behavior at the material level is typically described by a single constitutive law of the composite—defined by a stress versus deformation (σ-ε) or a stress versus crack opening (σ-w) relationship—which includes both the toughening contributions of the concrete matrix and that of the reinforcing fibers. This is the approach currently followed by the international design standards (ACI,[18] Model Code 2010,[19] RILEM Recommendations[20,21]), in which the FRC constitutive law is defined on the basis of experimental flexural tests by measuring the postcracking residual flexural strength at a given crack opening displacement.[22]

A similar design-by-testing procedure has been also applied by several investigators in different research works, in which an inverse procedure is applied to identify the global σ-w constitutive relationship starting from a load-deflection or a load-CMOD experimental curve.[23] This single constitutive law could also be used in a sectional model that is able, on the basis of equilibrium, constitutive, and kinematic conditions, to predict the flexural response of FRC and HRC elements.[24–28] Among these models, some of them were focused on the influence of fiber addition on the minimum reinforcement condition for HRC members.[26–28]

In all cases, the main drawback of the above-mentioned approach relies in the fact that the assumption of a single constitutive law for the fibrous composite—which is valid for a given percentage of reinforcing fibers, V_f—does not allow to capture the influence in the postcracking regime of each single constituent of the composite. As a direct consequence, these approaches do not permit to predict directly the transition in the flexural response due to the change in fiber volume fraction, V_f.

In the present work, the influence of steel-fiber addition on the flexural behavior of lightly RC members is discussed in the framework of fracture mechanics by means of the Bridged Crack Model.[29–40] The focus is on the *minimum reinforcement condition*, which is intended to be obtained when the ultimate moment is equal to the first cracking moment of the reinforced member.

The model, which was originally proposed for the case of steel-bar RC elements,[29–31] has been recently extended by the authors to the case of FRC[40–43] and HRC.[44,45]

2 | THE UPDATED BRIDGED CRACK MODEL

2.1 | Fundamentals

In the case of lightly- or fiber-reinforced concrete beams, the flexural response is mainly governed by the tensile cracking of the concrete member, which generally precedes concrete crushing at the compression edge (occurring for over-reinforced beams) as well as shear failure (occurring for deep beams). Under these circumstances, the following four regions can be identified in the critical cross-section of the specimen, where the damage is localized (see the left part of Figure 2): (i) ligament in compression; (ii) uncracked ligament in tension; (iii) reinforcement bridging zone, in which both short fibers and steel bars bridge the crack faces; (iv) stress-free crack zone, generally noticeable for large crack depths.

In this framework, the Updated Bridged Crack Model (UBCM) describes the crack propagation phenomenon by assuming that the tensile cracking precedes compression crushing and shear failure. The critical cross-section, where damage is localized, is assumed to have a rectangular shape, which is characterized by a thickness, b, a depth, h, an initial crack depth, a_0, and subjected to an external bending moment, M (see the central part of Figure 2).

The total number of reinforcing layers, each one characterized by its own position c_i, is given by the sum of steel-bar reinforcement layers, n_b, and reinforcing fibers crossing the crack, n_f. The quantity n_b is known a priori, whereas n_f is strictly related to the fiber distribution within the volume of the composite. The latter, n_f, can be calculated as:

$$n_f = \alpha V_f \frac{bh}{A_f}, \tag{1}$$

where A_f is the cross-sectional area of the single fiber, and α the orientation factor. The latter, which is defined as the ratio between the actual number of fibers in the critical cross-section and the theoretical one, can be experimentally found by investigating the specimen fracture surface at the end of the experimental tests or predicted on the basis of statistical tools able to model the fiber distribution within the volume of the specimen. Among the total number of reinforcement layers in the critical cross-section, some of them, m, can be considered as active since they connect the two crack faces.

The UBCM assumes the composite as a multiphase material, in which the cementitious matrix and the reinforcing layers represent its primary and secondary phases, both contributing to the global toughening of the structural element. The concrete matrix is assumed to be linear-elastic perfectly- brittle, considering other nonlinear contributions (in tensile and compression behaviors) as negligible.

Under these assumptions, a $r^{-1/2}$ stress singularity is considered at the crack tip (see the right part of Figure 2), which is characterized by a global stress-intensity factor, K_I:
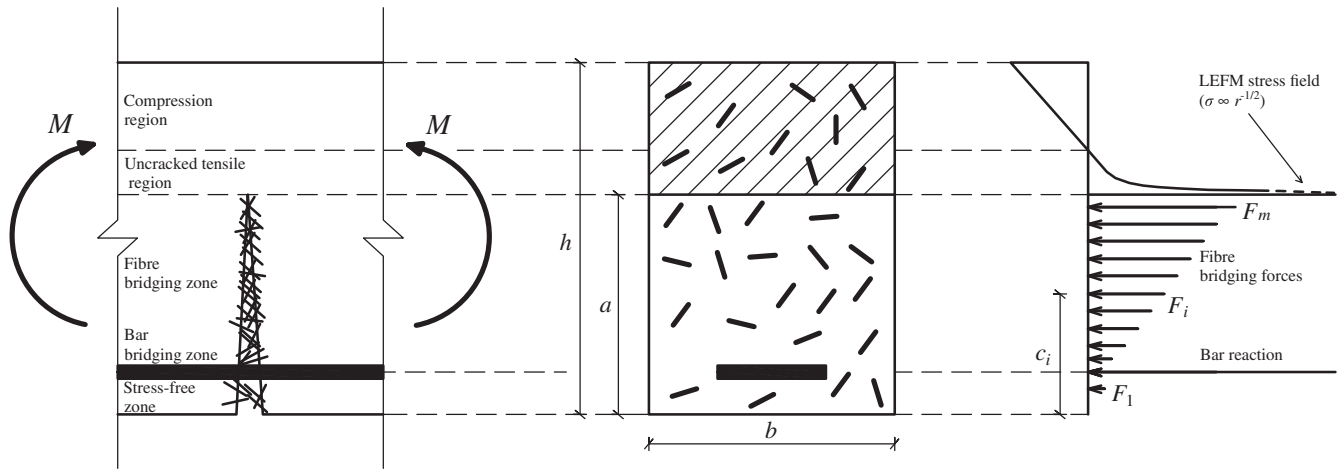
FIGURE 2 Critical cross-section in hybrid-reinforced concrete beam and stress distribution predicted by the Updated Bridged Crack Model.

$$K_I = K_{IM} - \sum_{i=1}^{m} K_{Ii} = \frac{M}{bh^{3/2}} Y_M - \frac{\{Y_F\}^T \{F\}}{bh^{1/2}}. \quad (2)$$

The crack propagation occurs when the stress-intensity factor, K_I, reaches its critical value, K_{IC}, that is, the fracture toughness of the plain matrix (unreinforced material). In Equation (2), both the contribution related to the applied bending moment, M, which tends to open the crack faces, and that related to the distribution of forces, $\{F\}$, which bridge the crack, appear.

The latter contribution represents the toughening action of the reinforcing secondary phase, which is described by a constitutive law of reinforcement. In the framework of fracture mechanics, it is defined in terms of stress versus crack opening displacement relationships, which can be generally written as:

for $i = 1, ..., n$

$$\sigma_i = f(w_i). \quad (3)$$

Equation (3) provides a set of n equations which relate the stress acting in the ith reinforcement, σ_i, with the corresponding crack opening displacement, w_i.

A hardening-perfectly plastic constitutive law (Figure 3) has been used to describe the yielding of the steel-bar[46]:

for $0 < w \leq w_y$:

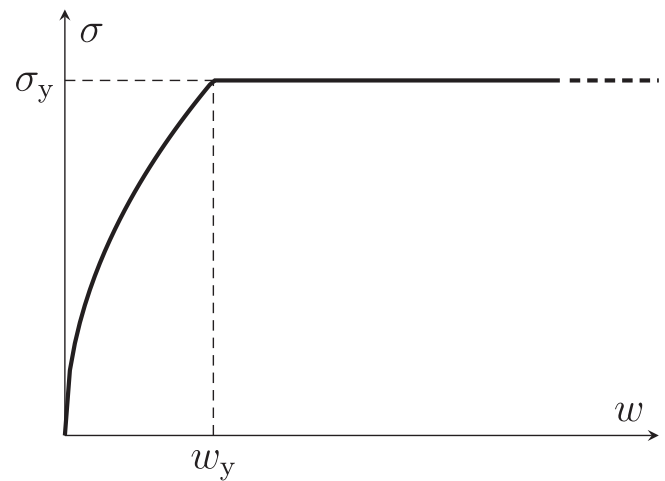$$\sigma_i(w_i) = \sigma_y \left(\frac{w_i}{w_y} \right)^{0.5}, \quad (4a)$$

for $w \geq w_y$:

FIGURE 3 Steel-bar hardening-perfectly plastic constitutive law.

$$\sigma_i(w_i) = \sigma_y, \quad (4b)$$

where σ_y is the yield strength and w_y the corresponding crack opening. The latter can be estimated as follows:

$$w_y = \frac{\sigma_y^2 \phi}{4 E_s \tau_m}, \quad (5)$$

where Φ is the steel-bar diameter, E_s is the steel-bar Young's modulus, and τ_m is the average shearing stress at the concrete-steel interface.

On the other hand, a rigid-softening constitutive law has been used to describe the slippage of the short fibers. Following the suggestions reported in the literature on the basis of experimental pull-out tests,[47–49] different softening laws need to be considered in the case of straight

FIGURE 4 Steel-fiber rigid-softening constitutive laws: (a) straight fiber; (b) hooked-end fiber.

$$\frac{\sigma}{\sigma_{\mathrm{s}}} = 1 - \left(\frac{w}{w_{\mathrm{c}}}\right)^{n}$$

(a)

$$\frac{\sigma}{\sigma_{\mathrm{s}}} = f\left(\frac{w}{w_{\mathrm{c}}}\right)$$

(b)
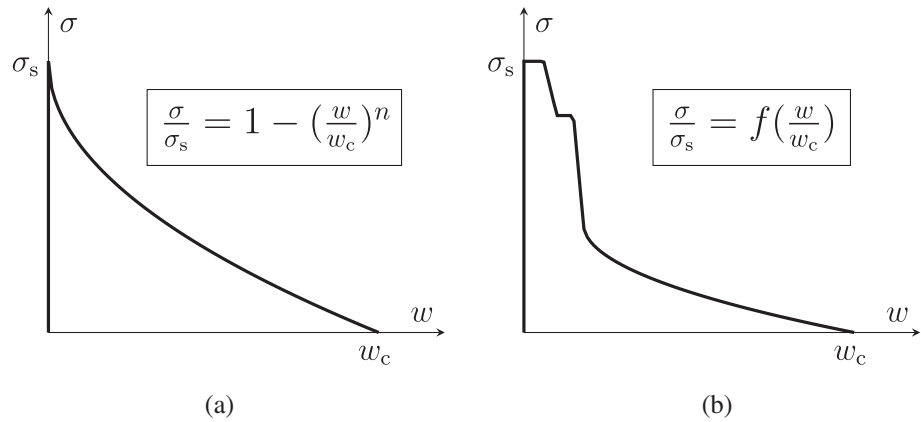
steel fibers and hooked-end steel fibers. In the case of a straight fiber, the pull-out behavior is well described by a descending power law (Figure 4a; $n = 0.5$). On the other hand, a piecewise function—indicated as f in Figure 4b—is suggested to describe the pull-out behavior of hooked-end fibers. The analytical expression of the piecewise function currently implemented in UBCM was recently defined by the authors in Accornero et al.[45] By keeping unchanged the shape of the bridging law, which is intended as a property of the fiber reinforcement, the related toughening contribution can be synthetically described by two parameters: (i) the slippage strength of the fiber, σ_{s}, beyond which the fiber pull-out is triggered; (ii) the fiber embedment length, w_{c}, beyond which the fiber bridging action is exhausted.

Finally, a set of compatibility conditions is needed to calculate the crack opening, w_i, at each ith active reinforcement level as a function of the applied bending moment, M, and of the bridging forces, F_i. In matrix form, we have:

$$\{w\} = \{\lambda_{\mathrm{M}}\}M - [\lambda]\{F\}, \tag{6}$$

where $\{w\}$ is the crack opening vector, $\{\lambda_{\mathrm{M}}\}$ is the vector of the local compliances due to the bending moment, and $[\lambda]$ is the matrix of the local compliances due to the bridging forces.

For a given crack depth, the problem relies in the determination of the $2m + 1$ unknowns, that is, the fracture moment, M_{F}, the profile of the crack opening displacements, $\{w\}$, and the corresponding distribution of bridging forces, $\{F\}$, related to both active steel bars and reinforcing fibers. The solution is obtained by means of a numerical iterative procedure based on the equilibrium (crack propagation) condition (Equation 2), on the reinforcement constitutive laws (Equation 3), and on the displacement compatibility conditions (Equation 6). It leads to the complete evaluation of the stress-profile represented in Figure 2.

Then, the local rotation of the HRC cross-section, φ, can be calculated as follows:

$$\varphi = \lambda_{\mathrm{MM}}M - \{\lambda_{\mathrm{M}}\}^{\mathrm{T}}\{F\}, \tag{7}$$

where λ_{MM} and $\lambda_{\mathrm{M},i}$ represent the local rotation due to a unit bending moment and to the ith bridging force, respectively. By virtue of Betti's Theorem, the coefficient $\lambda_{\mathrm{M},i}$ coincides with the ith crack opening, w_i, due to a unit bending moment (Equation 4).

The global deflection of the beam, δ, can be calculated by applying the superposition principle, according to which the total deflection takes into account both the nonlinear contribution related to the cracking process occurring at the critical section (inelastic hinge) and that related to the elastic behavior of the remaining part of the specimen. This approach, which is typically suggested in the case of cross-section models,[21] implies that the nonlinear features of the global response are restricted to the critical cross-section of the specimen, where the damage is assumed to be localized. The contribution related to the development and growth of multiple cracks along the beam specimen cannot be directly evaluated in the framework of UBCM, although it could be accounted for by introducing an equivalent inertia of the beam section.[50]

2.2 | Dimensionless numbers

Considering the shape of the reinforcement constitutive laws as a reinforcement property (Figures 3 and 4), the HRC sectional response is found to be governed by three scaling dimensionless numbers, that is, the *bar-reinforcement brittleness number*, N_{P}, the *fiber-reinforcement brittleness number*, $N_{\mathrm{P,f}}$, and the *pull-out brittleness number*, N_{w}:

$$N_{\mathrm{P}} = \rho \frac{\sigma_{\mathrm{y}}}{K_{\mathrm{IC}}} h^{1/2}, \tag{8}$$

$$N_{\mathrm{P,f}} = V_{\mathrm{f}} \frac{\alpha \sigma_s}{K_{\mathrm{IC}}} h^{1/2} = V_{\mathrm{f}} \frac{\overline{\sigma}_s}{K_{\mathrm{IC}}} h^{1/2}, \tag{9}$$

$$N_{\mathrm{w}} = \frac{E w_{\mathrm{c}}}{K_{\mathrm{IC}} h^{1/2}}. \tag{10}$$

The bar-reinforcement brittleness number, N_{P} (Equation 8), depends on the steel-bar reinforcement percentage, ρ, on the steel yield strength, σ_{y}, on the matrix fracture toughness, K_{IC}, as well as on the beam depth, h. An analogous expression (Equation 9) can be obtained for the fiber-reinforcement brittleness number, $N_{\mathrm{P,f}}$, by replacing the bar-reinforcement parameters, ρ and σ_{y}, with the fiber volume fraction, V_{f}, and the equivalent slippage strength of the fiber, $\overline{\sigma}_{\mathrm{s}}$, respectively. It should be noted that $\overline{\sigma}_{\mathrm{s}}$ takes into account the orientation factor, α. Finally, the pull-out brittleness number, N_{w} (Equation 10), depends on the equivalent embedded length of the fiber, w_{c}, on the matrix Young's modulus, E, on the matrix fracture toughness, K_{IC}, and on the beam depth, h.

It is worth emphasizing that these three brittleness numbers, N_{P}, $N_{\mathrm{P,f}}$, and N_{w}, encompass the influence of the single involved variables, such as the amount of the reinforcing phases and the structural size, in a comprehensive framework provided by UBCM. The influence of N_{P}, $N_{\mathrm{P,f}}$, and N_{w} on the flexural response of HRC beams is discussed in the next section.

3 | PARAMETRIC ANALYSIS AND MINIMUM REINFORCEMENT CONDITIONS

In this section, the cross-sectional response of a lightly HRC member is described in terms of dimensionless fracture moment, $\tilde{M}_{\mathrm{F}} = \frac{M_{\mathrm{F}}}{K_{\mathrm{IC}} b h^{3/2}}$, versus local rotation, $\tilde{\varphi} = \varphi \frac{E h^{1/2}}{K_{\mathrm{IC}}}$, as a function of the three brittleness numbers. The numerical results herein presented are obtained by considering a single layer of reinforcing steel-bar (Figure 3), which is placed at a distance from the beam intrados, c_0, equal to $0.15h$. In addition, hooked-end steel-fibers (Figure 4b) are considered as uniformly spaced within the concrete ligament. An initial notch, a_0, equal to the concrete cover is assumed ($a_0/h = c_0/h = 0.15$).

In Figure 5a, a family of curves is obtained by varying N_{P}, whereas the brittleness numbers related to the fiber-reinforcement, $N_{\mathrm{P,f}}$ and N_{w}, are kept unchanged ($N_{\mathrm{P,f}} = 0.20$; $N_{\mathrm{w}} = 1225$). It is evident how N_{P} governs the ductile-to-brittle transition in the whole postcracking

regime of the beam, thus providing a significant contribution in terms of global toughening and structural ductility/stability. In strong analogy to the case of FRC, which has been discussed by the authors in previous papers,[40–43] the numerical curves suggest to identify three stages being characterized by the flexural response of the HRC beam. In Stage I, the specimen exhibits a linear elastic behavior, until the first cracking moment (red square marker) is reached. At the onset of the fracturing process, the post-cracking regime takes place, which actually depends on the three dimensionless numbers. In the intermediate stage (Stage II) both steel bars and fibers contribute to the load bearing capacity (circle markers). In the final stage (Stage III), which describes the gradual exhaustion of the fiber toughening contribution, the curves tend towards different plastic plateaus, each one defined by its corresponding steel-bar reinforcement brittleness number, N_{P}.

The same discussion applies to the numerical curves of Figure 5b, where a variation in the fiber-reinforcement brittleness number, $N_{\mathrm{P,f}}$, affects just Stage II of the flexural response. Consistently with previous discussions, Stage III is characterized by an asymptotic convergence of all the curves to a common plastic plateau, which is defined by N_{P} (=0.10).

It is worth noting that even if the amount of steel-bar reinforcement, that is, N_{P}, is not sufficient to provide a stable postpeak response ($N_{\mathrm{P}} < N_{\mathrm{PC}} = 0.28$), the additional contribution represented by the reinforcing fibers, that is, $N_{\mathrm{P,f}}$, permits to obtain an ultimate bending moment greater than the first cracking moment (see the green, cyan, blue, and purple curves in Figure 5b). In this sense, the crucial point is that the minimum reinforcement condition in HRC beams, as defined before, can be obtained by an effective combination of N_{P} and $N_{\mathrm{P,f}}$.

Finally, the set of curves in Figure 5c is obtained by varying N_{w} and keeping unchanged the reinforcement brittleness numbers, N_{P} and $N_{\mathrm{P,f}}$ ($N_{\mathrm{P}} = 0.10$; $N_{\mathrm{P,f}} = 1.00$). N_{w} drives the decrement of the bearing capacity in the final stage (Stage III) toward the final plastic plateau of the response and, most importantly, does not affect the maximum load experienced by the specimen.

For each curve in Figure 5, both the first cracking moment (red square marker) and the ultimate bending moment (circle markers) can be evaluated, leading to define the minimum reinforcement conditions. The cracking moment can be calculated by means of Equation (2) by imposing $K_{\mathrm{I}} = K_{\mathrm{IC}}$, and considering that reinforcements are not active in the elastic stage of the response ($\{F\} = 0$). As a result, the dimensionless first cracking moment is solely a function of the initial notch depth, a_0/h: $\tilde{M}_{\mathrm{F}} = \frac{M_{\mathrm{F}}}{K_{\mathrm{IC}} b h^{3/2}} = \frac{1}{Y_{\mathrm{M}}(a_0/h)}$. On the other hand, a closed form expression cannot be found for the ultimate
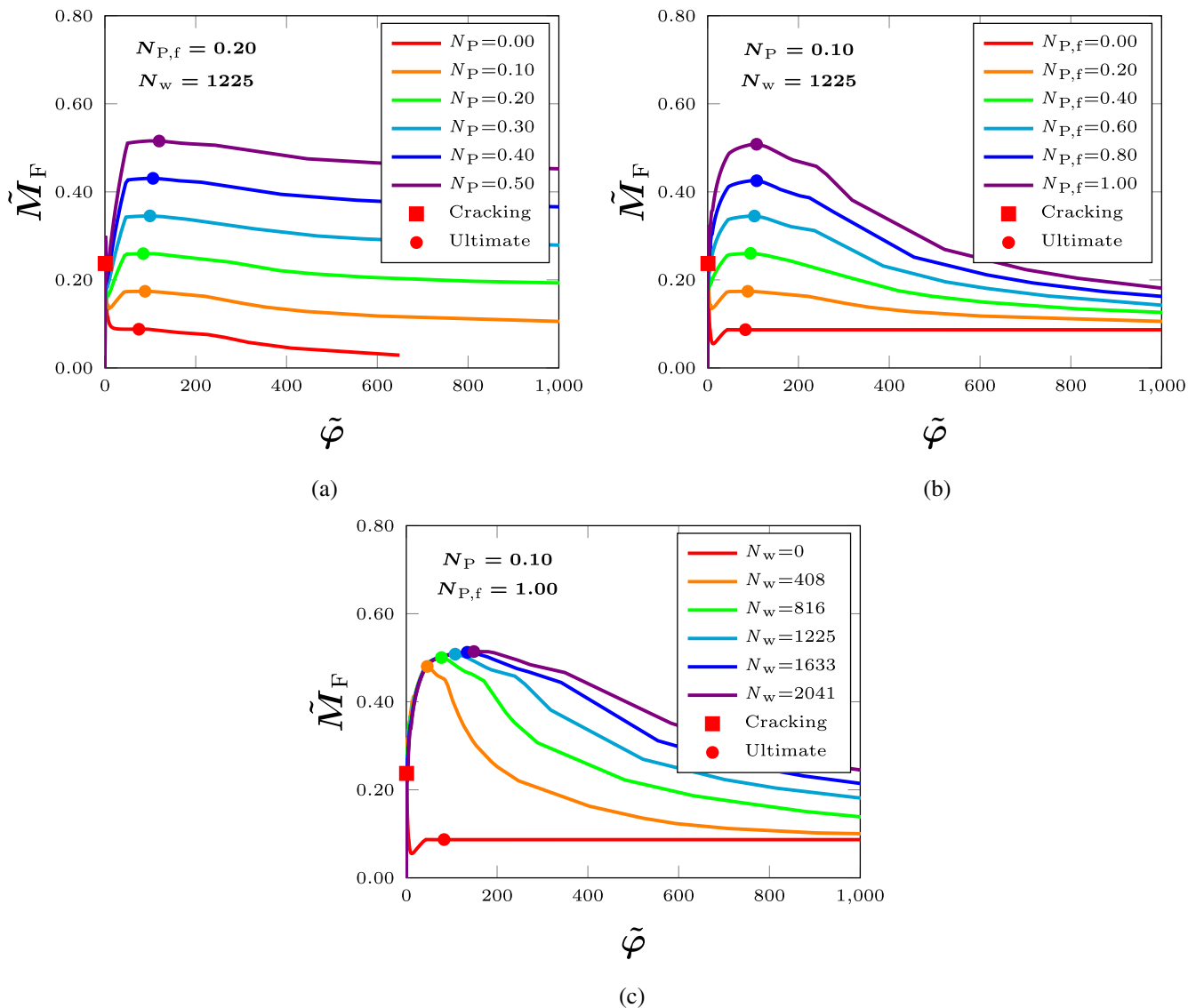
FIGURE 5 Dimensionless fracture moment versus local rotation of the hybrid-reinforced concrete beam: (a) influence of N_P; (b) influence of $N_{P,f}$; (c) influence of N_w.

bending moment, which actually depends on the reinforcement brittleness numbers, N_P and $N_{P,f}$, whereas the influence of N_w is negligible (see Figure 5).

Therefore, the minimum reinforcement conditions predicted by UBCM can be synthetically represented in a nomograph (Figure 6), where each blue point corresponds to a combination of the two reinforcement brittleness numbers, N_P and $N_{P,f}$, required to guarantee a stable post-peak response of the composite beam. Considering the whole set of numerical data (blue points), it is found that in the critical conditions N_P and $N_{P,f}$ can be effectively interpolated by a linear relation (red line), which defines the minimum reinforcement condition of HRC beams. In this sense, the regression curve works as a dividing line between two domains in the proposed
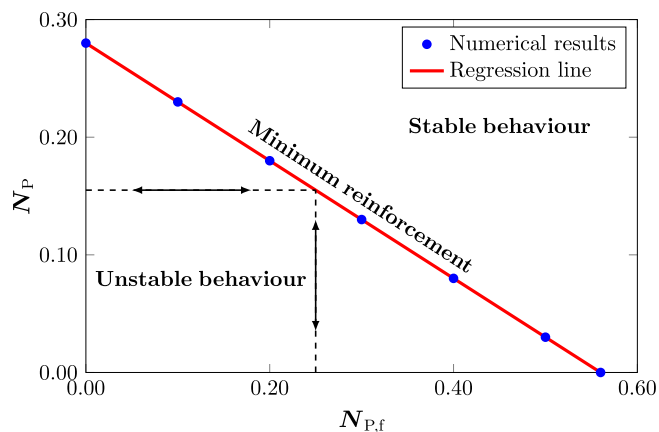

FIGURE 6 Minimum reinforcement design diagram for hybrid-reinforced concrete beams.

nomograph, for which the combination of N_P and $N_{P,f}$ provides a stable or unstable response, respectively. For a given value of N_P—that is, a certain percentage of steel-bar reinforcement, ρ—, it is possible to obtain the corresponding value of $N_{P,f}$—that is, the fiber volume fraction, V_f—required to guarantee the minimum reinforcement condition, and vice-versa (see dashed black arrows in Figure 6). Therefore, the diagram of Figure 6 can be used as an effective tool for a quantitative evaluation of the amount of reinforcing fibers necessary to a partial (or total) replacement of steel bars in HRC structures in flexure.

It is worth emphasizing that these predictions take into account the variation of some crucial parameters for the design of HRC members, such as the amount of the reinforcing phases, ρ and V_f, and the beam depth, h, which are englobed in the definition of the brittleness numbers, N_P, $N_{P,f}$, and N_w. Consistently with Equations (8), (9), an increase in ρ and/or V_f provides a proportional increase in the corresponding reinforcement brittleness numbers, N_P and/or $N_{P,f}$, leading to the ductile-to-brittle transition represented in Figure 5a,b, respectively.

An analogous trend occurs when h increases, whereby the related nonlinear increase in N_P and $N_{P,f}$ leads to a simultaneous increase in the load-bearing capacity (circle marker) and in the level of the final plastic plateau (horizontal asymptote), providing a greater stability to the flexural response. This trend has a direct effect on the HRC minimum reinforcement condition, which is found to be scale-dependent. In other words, for a given couple of critical values belonging to the regression line of Figure 6, N_P and $N_{P,f}$, it is found that $\rho_{min} \propto h^{-1/2}$ and $V_{f,min} \propto h^{-1/2}$, respectively.

Moreover, it should be noted that an increase in h provides also a reduction in N_w (Equation 10), corresponding to a quicker exhaustion of the fiber contribution in the final stage of the response, that is, a faster convergence of the flexural curves toward the final plastic plateau (Figure 5c).

4 | EXPERIMENTAL VALIDATION

In this section, an extensive experimental campaign recently carried out by Holschemacher et al.[51] is taken into consideration. Four-point bending tests were performed on high-strength concrete beams, characterized by a span of 600 mm, a thickness of 150 mm, and a depth of 150 mm, reinforced with steel bars and steel fibers. The concrete mixture was characterized by a 28-day average cubic compression strength of 86 MPa. Three different steel-fiber types are considered. Two hooked-end

steel-fiber types, F1 and F2, are characterized by the same geometry but different nominal tensile strengths, equal to 1100 and 1900 MPa, respectively. In addition, one corrugated steel-fiber type, F3, was tested. For each fiber type, four different fiber volume fractions were considered: 0, 20, 40, and 60 kg/m^3. On the other hand, three different steel-bar reinforcement percentages were adopted: 0.00%, 0.25% (2Φ6), and 1.00% (2Φ12).

In this work, only the results obtained in the case of fiber-type F1 are shown. In addition, the specimens with $\rho = 1.00\%$ are excluded from the present investigation due to the concrete crushing or shearing failure experienced by these specimens. Further information about the experimental testing can be found in Holschemacher et al.[51]

4.1 | Identification of the constitutive parameters

The application of the UBCM to HRC specimens requires the identification of the mechanical parameters of the matrix (concrete fracture toughness, K_{IC}), of the steel bar (yield strength, σ_y), and of the steel fibers (slippage strength, $\overline{\sigma}_s$, and the fiber embedment length, w_c). Therefore, an identification procedure is performed on the basis of the experimental tests carried out on plain concrete, RC, and FRC specimens.

The concrete fracture toughness, K_{IC}, has been identified by considering the peak load measured during the flexural tests carried out on plain concrete (experimental curve A-0 in Holschemacher et al.[51]). It is worth recalling that specimens A-0 were nominally unnotched. Under these circumstances, the application of UBCM requires the introduction of a fictitious initial notch, a_0/h, to define the load at the onset of the cracking process.

Considering the discussion in the previous section, a given value of the cracking load (moment) can be matched by means of different combinations of a_0/h and K_{IC}: $M_F = \frac{K_{IC}}{Y_M(a_0/h)} bh^{3/2}$. In this sense, in the case of unnotched specimens K_{IC} becomes a fictitious constitutive parameter of the concrete matrix, considering that for each value of a_0/h that is assumed, a different value of K_{IC} can be defined. In other words, the variation of these two parameters, $a_0/$ and K_{IC}, is balanced so that the experimentally observed cracking load is obtained. In addition, the constitutive parameters of the reinforcing phases are not affected by a_0/h since they refer to the post-cracking stage of the response. As a consequence, the features of the flexural response (cracking and ultimate loads, minimum reinforcement condition) are not affected by the choice of a_0/h, as recently discussed by the authors in a recent research work.[43] In the case under

investigation, a fictitious notch equal to the concrete cover is assumed ($a_0/h = c_0/h = 0.15$), leading to K_{IC} equal to 64 MPa mm$^{1/2}$.

The yielding stress of the steel bar, σ_y, has been identified by considering the level of the plastic plateau in the case of RC without steel fibers (experimental curve B-0 in Holschemacher et al.[14]). The corresponding crack opening, w_y, is calculated by means of Equation (5) considering the mechanical properties declared in Holschemacher et al.,[51] and it is found to be equal to 0.60 mm.

Eventually, by considering the bridging law for hooked-end steel fiber (Figure 4b), the related constitutive parameters, $\overline{\sigma}_s$ and w_c, have been identified by considering the flexural curve of the FRC specimens, without steel bars (experimental curves A-1, A-2, and A-3 in Holschemacher et al.[51]). The average values of the identified mechanical parameters are collected in Table 1.

4.2 | Prediction of the HRC flexural response

When the mechanical properties of each phase of the composite are identified, the flexural response of HRC specimens can be predicted as a function of the amount of the reinforcing phases, that is, the fiber volume fraction, V_f, and the steel-bar reinforcement percentage, ρ. The superposition between experimental data (dotted curves) and numerical predictions (continuous curves) is represented in Figure 7 for the specimens under investigation, characterized by $\rho = 0.25\%$, and V_f equal to 0 Kg/m^3 (curves B-0), 20 Kg/m^3 (curves B-20), 40 Kg/m^3 (curves B-40), and 60 Kg/m^3 (curves B-60). In all cases, a good agreement between numerical and experimental curves is obtained, together with an accurate evaluation of the cracking moment and of the ultimate bending moment of the HRC beams.

Within the framework of UBCM, these different behaviors can be synthetically described in terms of

brittleness numbers. It can be noted that, for given values of the mechanical properties, the variation in V_f affects $N_{P,f}$ according to Equation (9). $N_{P,f}$ is equal to 0, 0.22, 0.44, and 0.66 for specimens B-0, B-20, B-40, and B-60, respectively. On the other hand, N_P (=0.38) and N_w (=531) remain unchanged for all specimens, according to Equation (8) and Equation (10). In this sense, the influence of fibers on the response is consistently captured by the model, considering the greater load-bearing capacity of HRC specimens (curves B-20, B-40, B-60) with respect to ordinary RC (curves B-0).

Considering the stability of the flexural response, in all cases a stable postcracking response is experimentally observed (ultimate load greater than cracking load), since the amount of steel bar area was already sufficient to guarantee the minimum reinforcement condition regardless of the addition of steel fibers ($N_P = 0.38 > 0.28 = N_{PC}$).

By means of the design nomograph (Figure 6), the minimum reinforcement condition of the HRC beams—that is, the combination of ρ_{min} and $V_{f,min}$—can be predicted. Despite the minimum reinforcement can be described by any point of the regression line, for the sake
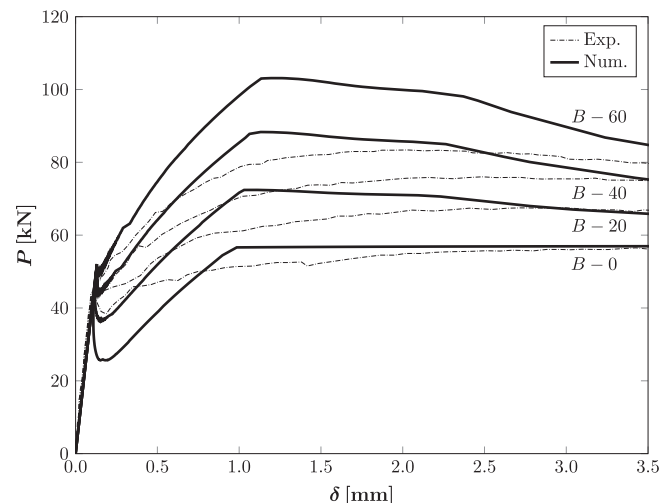

FIGURE 7 Prediction of the hybrid-reinforced concrete experimental curves.

TABLE 1 Identified mechanical properties.

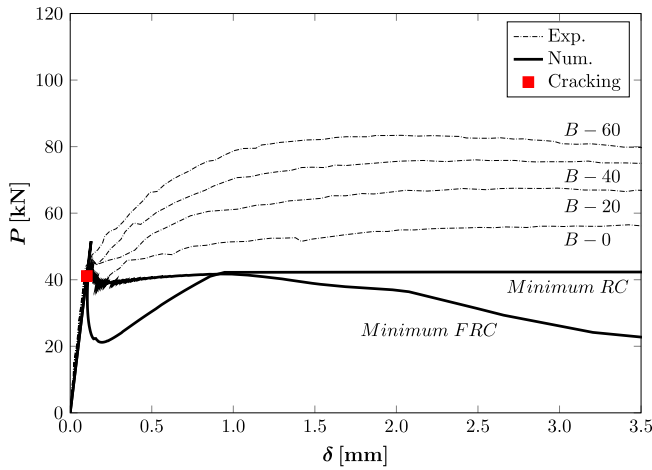| ID	Fiber-type	ρ (%)	$V_f \gamma_f$ (kg/m^3)	K_{IC} (MPa mm$^{1/2}$)	σ_y (MPa)	$\overline{\sigma}_s$ (MPa)	w_c (mm)
A-0	F1	0.00	0	64	–	–	–
B-0		0.25	0	–	800	–	–
A-1		0.00	20	–	–	524	12.5
A-2		0.00	40	–	–	454	9
A-3		0.00	60	–	–	408	9.5
Avg.	–	–	–	64	800	462	10

FIGURE 8 Prediction of the minimum reinforcement conditions.

of simplicity two limit conditions are taken into account. They correspond to the case of RC, in which the minimum reinforcement is obtained only by means of longitudinal steel bars, and to the case of FRC, in which the minimum reinforcement is given only by means of short steel fibers. In Figure 6, these two conditions correspond to two points given by the intersection of the regression line with the axes of the nomograph, and they are characterized by the coordinates $(0; N_P = 0.28)$ and $(N_{P,f} = 0.56; 0)$, respectively.

Considering the identified mechanical properties of the composite (Table 1), the two limit conditions correspond to ρ_{min} equal to 0.19%, and $V_{f,min}$ equal to 0.63%, respectively. The related UBCM numerical predictions are represented in Figure 8 (continuous thick lines), together with the experimental curves (dashed lines). The other critical conditions, which are defined by the other points of the regression line of Figure 6, lead to flexural curves included between the two previous ones.

5 | CONCLUSIONS

The minimum reinforcement condition in HRC beams is interpreted in the framework of fracture mechanics by means of the UBCM. The model assumes the reinforced element as a multi-phase composite, in which the cementitious matrix (primary phase) is assumed to be linear-elastic perfectly brittle. On the other hand, different nonlinear constitutive laws are used to model the behavior of the reinforcing phases, considering the yielding of the steel-bar reinforcements and the slippage of the short fibers.

The ductile-to-brittle transitions characterizing the structural behavior are governed by three scaling dimensionless numbers: the *bar-reinforcement brittleness*

number, N_P, which describes the toughening contribution of the steel-bar reinforcement; the *fiber-reinforcement brittleness number*, $N_{P,f}$, and the *pull-out brittleness number*, N_w, which both describe the toughening contribution of the reinforcing fibers. The minimum reinforcement condition in HRC structures is proven to be obtained by an effective combination of N_P and $N_{P,f}$.

The effectiveness of the model is discussed on the basis of a recent experimental campaign, in which the structural behavior of HRC beams is investigated. The substantial overlapping between numerical predictions and experimental results suggests the applicability of the model as a design-by-testing procedure to determine the minimum reinforcement conditions for HRC beams, thus promoting the fibers as an effective partial or total replacement of traditional steel bars.

NOTATION

A_f	fiber cross-section area
a	actual crack depth
a_0	initial crack depth
b	beam thickness
c_i	ith reinforcement layer position
c_0	concrete cover
E	concrete Young's modulus
E_s	steel-bar Young's modulus
F_i	ith bridging force
$\{F\}$	bridging forces vector
h	beam depth
K_I	stress-intensity factor
K_{IC}	concrete fracture toughness
K_{Ii}	stress-intensity factor due to the i-th bridging force
K_{IM}	stress-intensity factor due to the applied bending moment
M	applied bending moment
M_F	fracture moment
$\tilde{M}_F$	dimensionless fracture moment
m	number of active reinforcement layers in the cross-section
N_P	bar-reinforcement brittleness number
$N_{P,f}$	fiber-reinforcement brittleness number
N_{PC}	critical value of the reinforcement brittleness number
N_w	pull-out brittleness number
n_b	number of steel-bar reinforcement layers in the cross-section
n_f	total number of fibers in the cross-section
V_f	fiber volume fraction
$V_{f, min}$	minimum fiber volume fraction
w_i	ith crack opening displacement
$\{w\}$	crack opening displacements vector

w_c	critical crack opening at the fiber-reinforcement, or fiber embedment length
w_y	crack opening displacement at the steel-bar yielding
$\{Y_F\}$	bridging force shape function vector
Y_M	shape function due to the applied bending moment
α	orientation factor
φ	local rotation
$\tilde{\varphi}$	dimensionless local rotation
λ_{MM}	local rotation compliance
$[\lambda]$	matrix of the bridging force local compliances
$\{\lambda_M\}$	vector of the bending moment local compliances
ρ	steel bar area percentage
ρ_{min}	minimum steel bar area percentage
σ_i	ith bridging stress
σ_s	fiber slippage strength
$\overline{\sigma}_s$	equivalent fiber slippage strength
σ_y	steel yielding strength
τ_m	average shearing stress at the concrete-steel interface
Φ	steel-bar diameter

DATA AVAILABILITY STATEMENT

The data that support the findings of this study are available from the corresponding author upon reasonable request.

ORCID

Alessio Rubino https://orcid.org/0000-0002-7917-549X
Federico Accornero https://orcid.org/0000-0002-9638-8411

REFERENCES

1. Barros JOA, Sena Cruz J. Fracture energy of steel fiber-reinforced concrete. Mech Comp Mater Struct. 2001;8(1):29–45.
2. Mobasher B, Bakhshi M, Barsby C. Backcalculation of residual tensile strength of regular and high performance fiber reinforced concrete from flexural tests. Construct Build Mater. 2014;70:243–53.
3. Bencardino F, Rizzuti L, Spadea G, Swamy RN. Experimental evaluation of fiber reinforced concrete fracture properties. Vol 41, 1. Composites: Part B; 2010. p. 17–24.
4. Choi W-C, Jung K-Y, Jang S-J, Yun H-D. The influence of steel fiber tensile strengths and aspect ratios on the fracture properties of high-strength concrete. Materials. 2019;12(13):2105.
5. Yoo D-Y, Banthia N, Yang Y, Yoon Y-S. Size effect in normal- and high-strength amorphous metallic and steel fiber reinforced concrete beams. Construct Build Mater. 2016;121:676–85.
6. Lo Monte F, Ferrara L. Tensile behaviour identification in ultra-high performance fibre reinforced cementitious composites: indirect tension tests and back analysis of flexural test results. Mater Struct. 2020;53:145.
7. Altun T, Haktanir T, Ari K. Effects of steel fiber addition on mechanical properties of concrete and RC beams. Construct Build Mater. 2007;21(3):654–61.
8. Dancygier AN, Savir Z. Flexural behavior of HSFRC with low reinforcement ratios. Eng Struct. 2006;28(11):1503–12.
9. Ning X, Ding Y, Zhang F, Zhang Y. Experimental study and prediction model for flexural behavior of reinforced SCC beam containing steel fibres. Construct Build Mater. 2015;93:644–53.
10. Nguyen W, Bandelt MJ, Trono W, Billington SL, Ostertag CP. Mechanics and failure characteristics of hybrid fiber-reinforced concrete (HyFRC) composites with longitudinal steel reinforcement. Eng Struct. 2019;183:243–54.
11. Meda A, Minelli F, Plizzari GA. Flexural behaviour of RC beams in fibre reinforced concrete. Composites. 2012;43:2930–7.
12. Mertol HC, Baran E, Bello HJ. Flexural behavior of lightly and heavily reinforced steel fiber concrete beams. Construct Build Mater. 2015;98:185–3.
13. Shao Y, Billington SL. Flexural performance of steel-reinforced engineered cementitious composites with different reinforcing ratios and steel types. Construct Build Mater. 2020;231:117159.
14. Chunxiang Q, Patnaikuni I. Properties of high-strength steel fiber-reinforced concrete beams in bending. Cement Concrete Comp. 1999;21(1):73–81.
15. Fanella DA, Naaman AE. Stress-strain properties of fiber reinforced mortar in compression. ACI J. 1985;82(4):475–83.
16. Fantilli AP, Mihashi H, Vallini P. Post-peak behavior of cement-based materials in compression. ACI Mater J. 2007;104(5):501–10.
17. Campione G, La Mendola L. Behavior in compression of lightweight fiber reinforced concrete confined with transverse steel reinforcement. Cement Concrete Comp. 2004;26(6):645–56.
18. ACI (American Concrete Institute). *ACI 544.4R-18: guide to design with fiber-reinforced concrete*. Farmington Hills, MI: American Concrete Institute; 2019.
19. FIB – Federation International du Bèton. *Model Code 2010-Final Draft*. Switzerland, Lausanne, FIB Bull, p. 65. 2012.
20. RILEM TC 162-TDF. Test and design method for steel fibre reinforce concrete. σ-ε design method. Final recommendation. Mater Struct. 2003;36(8):560–7.
21. RILEM TC 162-TDF. Test and design method for steel fibre reinforce concrete. Design of steel fibre reinforced concrete using the σ-w method: principles and applications. Mater Struct. 2002;35(5):262–78.
22. Di Prisco M, Plizzari G, Vandewalle L. Fibre reinforced concrete: new design perspective. Mater Struct. 2009;42:1261–81.
23. Suárez F, Gálvez JC, Alberti MG, Enfedaque A. Fracture and size effect of PFRC specimens simulated by using a trilinear softening diagram: a predictive approach. Materials. 2021;14:3795.
24. Volpatti G, Martinez JA, Diaz JC, Zampini D. Advanced closed-form moment-curvature formulation for steel fiber-reinforced concrete members. Comp Struct. 2022;279:114755.
25. Barros JOA, Taheri M, Salehian H. A model to simulate the moment-rotation and crack width of FRC members reinforced with longitudinal bars. Eng Struct. 2015;100:43–56.
26. Gorino A, Fantilli AP. Scaled approach to designing the minimum hybrid reinforcement of concrete beams. Materials. 2020;13(22):5166.

27. Mobasher B, Yao Y, Soranakom C. Analytical solutions for flexural design of hybrid steel fiber reinforced concrete beams. Eng Struct. 2015;100:164–77.

28. Shao Y, Billington SL. Predicting the two predominant flexural failure paths of longitudinally reinforced high-performance fiber-reinforced cementitious composite structural members. Eng Struct. 2019;199:109581.

29. Carpinteri A. A fracture mechanics model for reinforced concrete collapse. Proceedings of the IABSE Colloquium on Advanced Mechanics of Reinforced Concrete, Delft, pp. 17–30. 1981.

30. Carpinteri A. Stability of fracturing process in RC beams. J Struct Eng ASCE. 1984;110(3):544–58.

31. Carpinteri A, Carpinteri A. Hysteretic behavior of RC beams. J Struct Eng ASCE. 1984;110(9):2073–84.

32. Bosco C, Carpinteri A. Discontinuous constitutive response of brittle matrix fibrous composites. J Mech Phys Solids. 1995; 43(2):261–74.

33. Carpinteri A, Massabò R. Bridged versus cohesive crack in the flexural behavior of brittle-matrix composites. Int J Fract. 1996; 81(2):125–45.

34. Carpinteri A, Massabò R. Continuous vs discontinuous bridged crack model of fiber-reinforced materials in flexure. Int J Solids Struct. 1997;34(18):2321–38.

35. Carpinteri A, Massabò R. Reversal in failure scaling transition of fibrous composites. J Eng Mech ASCE. 1997;123(2):107–14.

36. Carpinteri A, Puzzi S. The bridged crack model for the analysis of brittle matrix fibrous composites under repeated bending loading. J Appl Mech ASME Trans. 2007;74(6):1239–46.

37. Carpinteri A, Accornero F. The bridged crack model with multiple fibers: local instabilities, scale effects, plastic shake-down, and hysteresis. Theor Appl Fract Mech. 2019;104:102351.

38. Carpinteri A, Accornero F. Residual crack opening in fiber-reinforced structural elements subjected to cyclic loading. Strength Fract Complex. 2020;12(2–4):63–74.

39. Accornero F, Rubino A, Carpinteri A. Ductile-to-brittle transition in fiber-reinforced concrete beams: scale and fiber volume fraction effects. Mater Des Process Commun. 2020;2(6):1–11.

40. Rubino A, Accornero F, Carpinteri A. Post-cracking structural behaviour in FRC beams: scale effects and minimum fibre volume fraction. *Proceedings of the fib Symposium on Concrete Structures: New Trends for Eco-Efficiency and Performance*, Lisbon, 14–16 June 2021, pp. 622–631. 2021.

41. Accornero F, Rubino A, Carpinteri A. Post-cracking regimes in the flexural behaviour of fibre-reinforced concrete beams. Int J Solids Struct. 2022;248:111637.

42. Accornero F, Rubino A, Carpinteri A. Ultra-low cycle fatigue (ULCF) in fibre-reinforced concrete beams. Theor Appl Fract Mech. 2022;120:103392.

43. Carpinteri A, Accornero F, Rubino A. Scale effects in the post-cracking behaviour of fibre-reinforced concrete beams. Int J Fract. 2022;240:1–16.

44. Rubino A, Accornero F, Carpinteri A. Fracture mechanics approach to flexural behaviour of hybrid-reinforced concrete (HRC) beams. *Proceedings of the 6th fib Congress on Concrete Innovation for Sustainability*, Oslo, 12–16 June 2022, pp. 1670–1679. 2022.

45. Accornero F, Rubino A, Carpinteri A. A fracture mechanics approach to the design of hybrid-reinforced concrete beams. Eng Fract Mech. 2022;275:108821.

46. Ruiz G, Elices M, Planas J. Size effects and bond-slip dependence of lightly reinforced concrete beams. Eur Struct Integrity Soc. 1999;24:67–97.

47. Alwan JM, Naaman AE, Guerrero P. Effect of mechanical clamping on the pull-out response of hooked steel fibers embedded in cementitious matrices. Concrete Sci Eng. 1999;1(1):15–25.

48. Robins P, Austin S, Jones P. Pull-out behaviour of hooked steel fibres. Mater Struct. 2002;35:434–42.

49. Abdallah S, Rees DWA. Analysis of pull-out behaviour of straight and hooked end steel fibres. Engineering. 2019;11(6):332–41.

50. ACI (American Concrete Institute). ACI 318–19: building code requirements for structural concrete. Farmington Hills, MI: American Concrete Institute; 2019.

51. Holschemacher K, Mueller T, Ribakov Y. Effect of steel fibres on mechanical properties of high-strength concrete. Mater Des. 2010;31(5):2604–15.

AUTHOR BIOGRAPHIES

Alessio Rubino, DISEG, Politecnico di Torino, Turin, Italy. Email: alessio.rubino@polito.it.

Federico Accornero, College of Engineering, Shantou University, Shantou, China. Email: federico@stu.edu.cn.

Alberto Carpinteri, Department of Civil and Environmental Engineering, Shantou University, Shantou, China. Email: alberto.carpinteri@polito.it.